



1 **Macroalgal influence on particulate organic matter sources and early transformation in an**  
2 **Arctic fjord**

3 Ashok S Jagtap<sup>1</sup>, Archana Singh<sup>1</sup>, Anand Jain<sup>1</sup>, Nandini Raj<sup>2</sup>, Manish Tiwari<sup>1</sup>

4 <sup>1</sup>National Centre for Polar and Ocean Research, Ministry of Earth Sciences, Vasco-da-Gama,  
5 Goa 403804, India

6 <sup>2</sup>Amity Institute of Biotechnology, Amity University, Uttar Pradesh 201313, India

7

8 Correspondence to:

9 Ashok S. Jagtap ([ashokjagtap200@gmail.com](mailto:ashokjagtap200@gmail.com)),

10 Archana Singh ([archanasingh@ncpor.res.in](mailto:archanasingh@ncpor.res.in))

11

12

13

14 **Highlights**

- 15 • Surface POM over macroalgal beds was observed enriched in labile carbon and nitrogen  
16 compounds.
- 17 • Monosaccharide and amino acid fingerprints revealed a macroalgal imprint on POM.
- 18 • Macroalgal-derived POM was exported and selectively transformed across fjord-scale  
19 gradients.
- 20 • Multivariate analysis (PCA) identified a continuous macroalgal–pelagic biogeochemical  
21 gradient.

22

23



24 **Abstract**

25 Accelerated Arctic warming is promoting the expansion of coastal macroalgal habitats, yet their  
26 influence on pelagic organic carbon cycling remains unresolved. This study investigate the  
27 influence of macroalgal beds on the biochemical composition of surface particulate organic matter  
28 (POM) in Kongsfjorden, Svalbard, during late summer 2023. Surface waters were sampled at four  
29 macroalgal-dominated sites (MDS) and from adjacent waters (Adj-W) located 500 m and 1500 m  
30 away. A multi-proxy approach integrating elemental composition, stable isotopes, biopolymeric  
31 fractions, monosaccharides, and amino acids was used to trace macroalgal contributions and their  
32 lateral redistribution. Concentrations of particulate organic carbon, particulate nitrogen, particulate  
33 carbohydrates, and proteins were consistently higher at MDS than in Adj-W, indicating localized  
34 enrichment of biochemically labile organic matter within macroalgal habitats. Molecular analyses  
35 revealed elevated concentrations of monosaccharides and amino acids at MDS, including  
36 macroalgal-associated sugars (glucose, galactose, fucose, mannuronic acid) and labile amino acids  
37 (Asp, Glu, Gly, Ser, Ala), demonstrating incorporation of macroalgal-bed derived matter into  
38 surface POM. Declining concentrations and composition shift in Adj-W, together with internal  
39 reorganization of biopolymeric and molecular composition, indicate efficient lateral export with  
40 selective early-stage transformation of POM. Bulk  $\delta^{13}\text{C}$  showed minimal spatial variation ( $-26.8$   
41 to  $-29.1\%$ ), suggesting that macroalgal influence is expressed through biochemical restructuring  
42 rather than isotopic dominance. Principal component analysis identified a continuous macroalgal–  
43 pelagic gradient, with MDS occupying the macroalgal-influenced end. Overall, these findings  
44 indicate that Arctic macroalgal beds act as dynamic coastal biogeochemical hotspot, redistributing  
45 and transforming organic carbon beyond their immediate habitat.



46 **Keywords:** Arctic fjords; macroalgal-derived organic matter; benthic–pelagic coupling; coastal  
47 carbon cycling; lateral transport

48

## 49 **1. Introduction**

50 Accelerated warming of the Arctic has led to pronounced environmental changes, including a  
51 reduction in sea ice extent and thickness, intensified glacier melt, widespread permafrost thawing,  
52 and a shift toward more liquid precipitation (Dai et al., 2019; Rantanen et al., 2022). These changes  
53 are altering marine primary production (Attard et al., 2024), coastal carbon sources (Mathew et al.,  
54 2025), and nutrient dynamics within Arctic fjord systems (McGovern et al., 2020). Amid these  
55 environmental transformations, macroalgae have demonstrated ecological resilience and  
56 adaptability, enabling their expansion along Arctic coastlines (Assis et al., 2022). Recent estimates  
57 of species distribution modeling indicate a substantial increase in subtidal (45%) and intertidal  
58 (8%) brown macroalgal cover along the Arctic coastline over the past few decades (Krause-Jensen  
59 et al., 2020). This rapid and ongoing macroalgal expansion contributes substantially to coastal  
60 primary productivity and carbon dynamics in the Arctic (Attard et al., 2024; Krause-Jensen et al.,  
61 2020). Macroalgal biomass and condition are strongly shaped by local environmental variability,  
62 with runoff and site-specific forcing influencing kelp biochemistry and ecosystem functioning in  
63 Arctic coastal systems (Castro de la Guardia et al., 2025; Niedzwiedz et al., 2025). Comparable  
64 environment-driven changes in kelp biomass and distribution have been reported across the Arctic,  
65 including Greenland and the Canadian Arctic, indicating pan-Arctic rather than site-specific  
66 responses (Carlson et al., 2026; Filbee-Dexter and Wernberg, 2020; Krause-Jensen and Duarte,  
67 2016). Kelp forest structure shifted markedly, with reduced depth distribution, declining  
68 abundance of several kelp species, and increasing dominance of *Alaria esculenta*, driven primarily



69 by rising turbidity and coastal darkening rather than temperature alone, thereby reshaping kelp  
70 biomass, demography, and ecosystem functioning in Kongsfjorden (Düsedau et al., 2024). Field  
71 experiments have also shown that macroalgal blades can lose approximately 3% of their total area  
72 per day, providing a substantial and continuous input of macroalgal-derived material to the coastal  
73 particulate organic matter (POM) pool (Buchholz and Wiencke, 2016).

74 Macroalgal beds contribute a significant amount of macroalgal-derived organic carbon,  
75 approximately 60% as particulate organic carbon (POC), and approximately 30% as dissolved  
76 organic carbon (DOC) (Kennedy and Blain, 2025; Pessarrodona et al., 2022) to the surrounding  
77 environment, and play a crucial role in supporting secondary production via detrital food web and  
78 coastal Arctic carbon cycling (Pedersen et al., 2021; Renaud et al., 2015; Simpkins et al., 2025).  
79 Macroalgal POM appears in multiple forms, whole thalli and tissue fragments, and is often buoyant  
80 due to structural features such as pneumatocysts, allowing particles to stay suspended in surface  
81 waters (Carlson et al., 2026; Kennedy and Blain, 2025). This buoyancy promotes extensive lateral  
82 transport across coastal and fjord systems, effectively linking benthic macroalgal production with  
83 pelagic environments and shaping the spatial distribution of the organic carbon (Carlson et al.,  
84 2026; van der Mheen et al., 2024). A substantial fraction of the carbon produced in macroalgal  
85 beds is exported to surrounding environments, with only about 2% remaining and settling at the  
86 site of production (Kennedy and Blain, 2025; Krause-Jensen and Duarte, 2016; Pessarrodona et  
87 al., 2022). Macroalgal POM undergoes microbial mediated transformation and degradation during  
88 transit and thereby affects biogeochemical processes in macroalgal beds as well as adjacent waters  
89 (Adj-W) (Duarte et al., 2013; Krause-Jensen and Duarte, 2016; Ortega et al., 2019). Biochemical  
90 compositional and lipid biomarker studies have shown hints of macroalgal contribution to POM  
91 (Singh et al., 2024b) and sediments (Roy et al., 2025) in Kongsfjorden. However, the magnitude



92 of macroalgal-derived organic carbon contributing to POM, and how this contribution varies  
93 spatially across coastal gradients away from macroalgal beds, remains poorly understood.

94 To resolve the sources and transformation pathways better, and to understand how the  
95 expansion of macroalgal forests will influence Arctic coastal biogeochemistry, a systematic  
96 biochemical characterization of POM in and around macroalgal-dominated sites is necessary.  
97 Thus, the present study investigated the biochemical composition of POM from the surface waters  
98 of Kongsfjorden (Svalbard) at four macroalgal-dominated sites (MDS), and at their respective  
99 adjacent waters (Adj-W) located 500 m and 1500 m from MDS sites. Here, we addressed two key  
100 questions: (i) *To what extent do the biochemical characteristics of surface POM at MDS reflect*  
101 *inputs from macroalgal-derived organic matter?* (ii) *How does the biochemical composition of*  
102 *POM change from MDS to Adj-W, and (iii) What do these changes reveal about the lateral*  
103 *transport and early alteration of macroalgal-derived organic matter?*

104

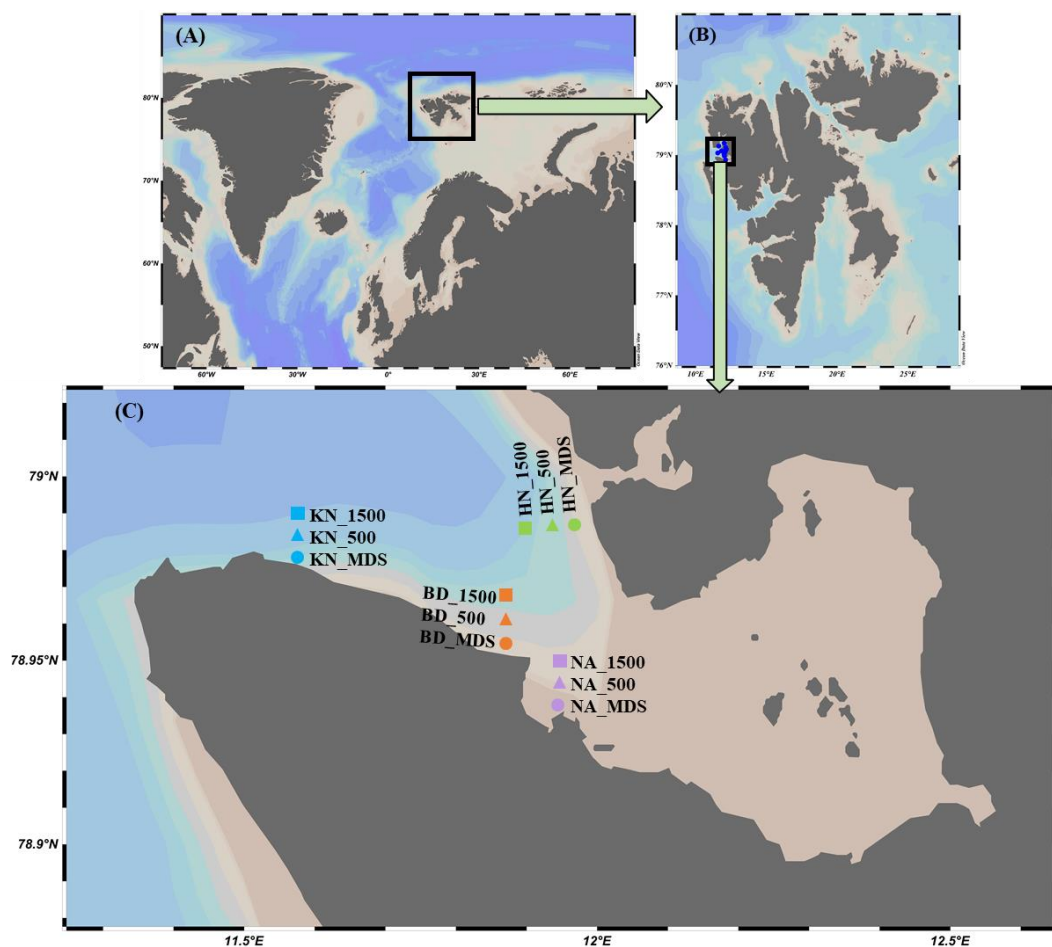
## 105 **Material and Methods**

### 106 **2.1 Sampling site and locations**

107 Surface water samples were collected during late summer 2023 (September–October) from four  
108 MDS distributed along and across the Kongsfjorden coast using the workboat Teisten, with a  
109 Niskin sampler deployed at 3 m depth, as well as from adjacent locations (Adj-W) located 500 m  
110 and 1500 m away from each MDS site (Figs. 1A-C). The seawater was prefiltered using a 200 µm  
111 mesh to remove larger particles. Seawater samples (3 L) were filtered using pre-combusted (4  
112 hours at 450 °C) 0.7 µm pore size glass fibre filters (GF/F) to collect particulate matter.  
113 Immediately after filtration, the GF/F filters were stored at -80 °C until analysis. An aliquot of 100



114 mL seawater sample for dissolved nutrients analysis was collected in high-density polyethylene  
115 bottles from each sampling location and stored at  $-80^{\circ}\text{C}$  until analysis.



116

117 **Figure 1.** Study area and sampling locations in the Arctic fjord system. (A) Regional map showing  
118 the broader Arctic context, (B) zoomed view of the fjord region, and (C) detailed map of sampling  
119 stations across nearshore macroalgal bed (MDS), mid-fjord (500 m), and offshore (1500 m) sites  
120 at BD, NA, KN, and HN.

121



## 122 **2.2 Physicochemical characteristics of seawater**

123 The vertical profiles of temperature, salinity, and turbidity at each sampling location were recorded  
124 using an SBE 911 plus instrument (Seabird Electronics Inc., USA). The concentrations of  
125 dissolved nutrients (nitrate, nitrite, silicate, and phosphate) were determined using a Seal AA3  
126 analytical Auto-analyser with a standard deviation of  $\pm 1\%$  and an  $R^2$  value of  $>0.99$  (Grasshoff et  
127 al., 2009). Chlorophyll *a* was extracted following (Singh et al., 2024a) with minor modifications.  
128 Briefly, GF/F filters were extracted in 90% acetone under low light conditions by keeping  
129 overnight at  $-20\text{ }^\circ\text{C}$ . The pigment extracts were centrifuged ( $10,000\times g$ ,  $4\text{ }^\circ\text{C}$ , 10 min), filtered ( $0.2$   
130  $\mu\text{m}$  PVDF), and analyzed using an Agilent 1200 HPLC with a ZORBAX 300 Extend-C8 column  
131 ( $1.1\text{ mL min}^{-1}$ ,  $40\text{ }^\circ\text{C}$ ). Pigments were separated using a reverse-phase methanol–ammonium  
132 acetate gradient and identified by comparing retention times and absorption spectra ( $250\text{--}850\text{ nm}$ )  
133 against DHI chlorophyll-*a* standard.

134

## 135 **2.3 Elemental and isotopic analyses of POM**

136 Filters containing particulate matter were dried at  $45\text{ }^\circ\text{C}$  for 24 h, after which carbonates were  
137 removed by exposing the filters to fumes of 35% HCl for 6 h in a desiccator. The treated filters  
138 were then weighed and tightly packed into tin capsules for elemental and isotopic analyses (Jain  
139 et al., 2019; Singh et al., 2024b). Particulate nitrogen (PN), particulate organic carbon (POC),  $\delta^{13}\text{C}$ -  
140 POC, and  $\delta^{15}\text{N}$ -PN were measured at the Marine Stable Isotope Laboratory, National Centre for  
141 Polar and Ocean Research, Goa, India, using an elemental analyser coupled to an isotope ratio  
142 mass spectrometer (EA-IRMS; Isoprime Vario Isotope Cube) operated in continuous-flow mode.  
143 External analytical precision for  $\delta^{13}\text{C}$  and  $\delta^{15}\text{N}$  was  $\pm 0.10\text{‰}$  and  $\pm 0.14\text{‰}$  ( $1\sigma$ ), respectively,  
144 determined by repeated analysis of caffeine (IAEA-600) and ammonium sulphate (IAEA-N1)



145 standards.  $\delta^{13}\text{C}$  and  $\delta^{15}\text{N}$  values are reported relative to VPDB and Air-N<sub>2</sub>, respectively, with  
146 ammonium sulphate (IAEA-N1) used for normalization to Air-N<sub>2</sub>. External precision for %C and  
147 %N was  $\pm 0.96\%$  and  $\pm 0.95\%$  ( $1\sigma$ ), respectively, based on repeated measurements of  
148 sulfanilamide.

149

#### 150 **2.4 Biochemical analysis of POM**

151 The dried and pre-weighed filters with POM were cut into smaller pieces using clean stainless  
152 steel scissors and then used for further analysis. The total particulate carbohydrates (P-CHO),  
153 particulate proteins (P-PRT), and particulate lipids (P-LIP) were analyzed using the phenol-  
154 sulfuric acid (Dubois et al., 1956), Lowry (Upreti et al., 1988), and Phospho-Vanillin (Folch et al.,  
155 1957) methods, respectively, and as described earlier in (Singh et al., 2024b). Biopolymeric carbon  
156 (BPC) was determined as depicted by (Danovaro et al., 2001), using the sum of the carbon  
157 equivalents of P-CHO, P-PRT, and P-LIP (conversion factors of 0.4, 0.49 and 0.75, respectively).

158

#### 159 **2.5 Monosaccharide composition analysis of POM**

160 For monosaccharide analysis, POM samples were acid-hydrolyzed and then analysed using High-  
161 performance Anion Exchange Chromatography coupled with Pulsed Amperometry Detector  
162 (HPAEC-PAD) as described earlier by (Singh et al., 2024a). In brief, GF/F filters with POM were  
163 treated with 1 mL of 12 M H<sub>2</sub>SO<sub>4</sub> at 25 °C for 2 h, diluted to 1.2 M with Milli-Q water, purged  
164 with N<sub>2</sub>, sealed, and incubated at 100 °C for 4 h. After cooling, internal standard (myo-inositol)  
165 was added and samples were neutralised with pre-combusted CaCO<sub>3</sub>, centrifuged (6000 rpm, 10  
166 min), and filtered (0.22  $\mu\text{m}$  PTFE). The samples were analysed using HPAEC-PAD (Metrohm  
167 940 Professional IC Vario) equipped with a Au-working electrode and Ag/AgCl reference



168 electrode, on a Metrosep Carb 2 (250/4.0) coupled with guard column at 30 °C. Sugars were  
169 separated using gradient elution (0.6 mL min<sup>-1</sup>) with solvent A (1 mM NaOH, 1 mM sodium  
170 acetate) and solvent B (150 mM NaOH, 100 mM sodium acetate) over 120 min. Neutral, amino  
171 sugars, and mannitol were resolved isocratically with solvent A, while acidic sugars were separated  
172 using the solvent B gradient. Identification and quantification of monosaccharides were achieved  
173 using calibration with a mixture of sugar standards (Sigma).

174

## 175 **2.6 Amino acid composition analysis of POM**

176 For amino acid analysis, POM samples were acid-hydrolyzed using HCl and then analysed using  
177 High-Performance Liquid Chromatography coupled with Diode Array Detector (HPLC-DAD)  
178 using method outlined by (Kim et al., 2024). GF/F filters with POM were cut into small pieces,  
179 placed in Pyrex tubes with 10 mL of 6 M HCl, purged with N<sub>2</sub>, sealed, and hydrolysed at 110 °C  
180 for 22 h. After cooling, nor-leucine was added as an internal standard. The hydrolysate was  
181 centrifuged, freeze-dried, reconstituted in 1 mL Milli-Q water, vortexed, and filtered (0.22 µm).  
182 Amino acids were derivatised by sequentially mixing 2.5 µL borate buffer with 1 µL sample (0.5  
183 min), followed by addition of 1 µL OPA reagent, mixing, and dilution with 15.5 µL Milli-Q water  
184 in HPLC (Agilent 1200) autosampler prior to injection. HPLC separation of the derivatized amino  
185 acids was carried out using a Zorbax AAA column (5 µm, 4.6 × 150 mm), a 20 µL injection  
186 volume, and a flow rate of 2 mL min<sup>-1</sup>. Detection was performed using a DAD (Agilent) at 338  
187 nm (reference 390 nm). The separation was carried out using a gradient elution with mobile phase  
188 A (40 mM phosphate buffer, pH 8.2) and mobile phase B (acetonitrile: methanol: water, 45:45:10).  
189 Identification and quantification were performed using external calibration with a 17 amino acid  
190 standard mixture (10, 100, 250, 1000 pmol, Agilent, USA).



191

## 192 **2.7 Statistical analysis**

193 Pearson correlation analysis at a significance level of 0.05 was conducted in R 4.5.0 to examine  
194 the relationship between the variables. To minimize the dataset's dimensionality and identify the  
195 most prevalent patterns in the composition of POM, principal component analysis (PCA) was  
196 employed. Analysis of variance (ANOVA) was used to test for significant differences in POM  
197 composition between the MDS and Adj-W sites.

198

## 199 **3. Results**

### 200 **3.1 Salinity, temperature, nutrients and chl-a**

201 Surface seawater salinity exhibited spatial variation, with the lowest salinity ( $27.4 \pm 0.0$  psu)  
202 recorded at NA\_1500 station, a site most influenced by glacier meltwater, and the highest salinity  
203 ( $31.6 \pm 0.1$  psu) observed at KN\_MDS, the outermost site under the influence of oceanic circulation  
204 (Table 1). Surface seawater temperature was lowest ( $4.2 \pm 0.0$  °C) at NA\_500 and highest at  
205 KN\_MDS ( $5.5 \pm 0.0$  °C). The lowest turbidity ( $2.1 \pm 0.1$  NTU) was recorded at both BD\_MDS and  
206 HN\_MDS, while maximum turbidity ( $7.4 \pm 0.0$  NTU) was observed at KN\_MDS.

207 Nitrate varied from  $0.05 \mu\text{M}$  (BD\_MDS) to  $0.80 \mu\text{M}$  (NA\_1500) and showed an increasing  
208 trend from MDS toward Adj-W for NA, BD and HN (Table 1). The overall average nitrate  
209 concentrations were lower in MDS ( $0.39 \pm 0.23 \mu\text{M}$ ) compared to Adj-W ( $0.56 \pm 0.13 \mu\text{M}$ ).  
210 Comparing different stations, the average nitrate concentration of all NA stations were highest  
211 ( $0.66 \pm 0.12 \mu\text{M}$ ), followed by KN ( $0.53 \pm 0.10 \mu\text{M}$ ), HN ( $0.51 \pm 0.08 \mu\text{M}$ ), and lowest at BD stations  
212 ( $0.30 \pm 0.22 \mu\text{M}$ ). Nitrite concentration showed a similar pattern, with an increasing pattern from



213 MDS to Adj-W sites. However, phosphate concentrations showed minor differences (0.01 to 0.02  
 214  $\mu\text{M}$ ) among MDS and Adj-W sites.

215 Chlorophyll *a* (Chl *a*) concentrations ranged from  $0.04 \mu\text{g L}^{-1}$  to  $0.18 \mu\text{g L}^{-1}$  across all  
 216 stations (Table 1). Similar to nitrate, Chl *a* showed an increasing trend from MDS toward Adj-W  
 217 sites at NA, BD, and HN stations, while KN exhibited relatively low concentrations at both MDS  
 218 and Adj-W sites. Overall, the average Chl *a* concentration was lower at MDS ( $0.07 \mu\text{g L}^{-1}$ )  
 219 compared to Adj-W ( $0.08 \mu\text{g L}^{-1}$ ). Among stations, BD stations recorded the highest average Chl  
 220 *a* concentrations ( $0.11 \mu\text{g L}^{-1}$ ), followed by HN and NA with  $0.07 \mu\text{g L}^{-1}$ , whereas KN ( $0.04 \mu\text{g}$   
 221  $\text{L}^{-1}$ ) stations exhibited the lowest average concentrations.

222

223 **Table 1.** Station locations and measured physicochemical parameters (temperature, salinity,  
 224 nutrients, and chlorophyll *a*) across sampling stations

Station	Station depth [m]	Temp [°C]	Sal [PSU]	Turbidity [NTU]	Nitrate ( $\mu\text{M}$ )	Phosphate ( $\mu\text{M}$ )	Nitrite ( $\mu\text{M}$ )	Chlorophyll <i>a</i> [ $\mu\text{g L}^{-1}$ ]
NA_MDS	3.5	$5.0 \pm 0.1$	$31.3 \pm 0.0$	$3.5 \pm 0.4$	0.58	0.18	0.09	0.09
NA_500	122	$4.2 \pm 0.0$	$30.1 \pm 1.3$	$5.0 \pm 0.1$	0.61	0.17	0.11	0.04
NA_1500	300	$5.2 \pm 0.1$	$27.4 \pm 0.0$	$2.9 \pm 0.4$	0.80	0.20	0.11	0.08
BD_MDS	6.7	$5.1 \pm 0.0$	$29.9 \pm 0.0$	$2.1 \pm 0.1$	0.05	0.13	0.01	0.09
BD_500	146	$4.7 \pm 0.3$	$30.3 \pm 0.1$	$2.9 \pm 0.1$	0.39	0.15	0.04	0.18
BD_1500	362	$5.4 \pm 0.0$	$30.9 \pm 0.6$	$4.4 \pm 0.3$	0.45	0.15	0.06	0.05
KN_MDS	3.4	$5.5 \pm 0.0$	$31.6 \pm 0.1$	$7.4 \pm 0.0$	0.49	0.14	0.06	0.05
KN_500	216	$5.0 \pm 0.5$	$29.5 \pm 0.1$	$3.1 \pm 0.4$	0.65	0.16	0.08	0.06
KN_1500	240	$4.5 \pm 0.0$	$29.8 \pm 0.0$	$2.9 \pm 0.1$	0.45	0.14	0.07	0.05
HN_MDS	4.5	$4.5 \pm 0.2$	$28.7 \pm 1.8$	$2.1 \pm 0.1$	0.43	0.14	0.04	0.06
HN_500	76	$4.3 \pm 0.0$	$29.8 \pm 0.0$	$3.8 \pm 1.7$	0.58	0.13	0.05	0.06
HN_1500	315	$4.3 \pm 0.0$	$29.8 \pm 0.3$	$3.8 \pm 0.5$	0.52	0.13	0.07	0.09

225



226

### 227 **3.2 Elemental and stable isotopic composition**

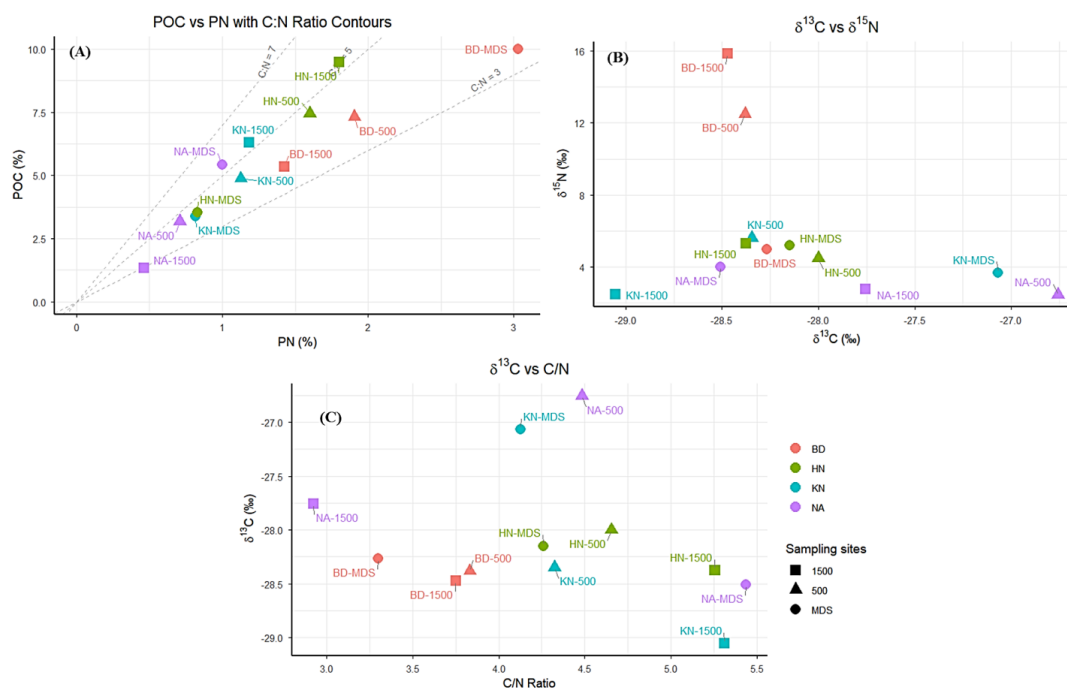
228 POC and PN concentrations varied in a wide range from 0.17 mg L<sup>-1</sup> (KN\_500) to 0.45 mg L<sup>-1</sup>  
229 (BD\_MDS) and from 0.04 mg L<sup>-1</sup> (KN\_500 and KN\_1500) to 0.14 mg L<sup>-1</sup> (BD\_MDS),  
230 respectively (Fig. 2A). BD\_MDS recorded the highest POC concentration (0.45 mg L<sup>-1</sup>), followed  
231 by NA\_MDS and HN\_MDS (0.32 mg L<sup>-1</sup>), with the lowest POC at KN\_MDS (0.21 mg L<sup>-1</sup>).  
232 Overall average POC and PN concentrations were higher at MDS (0.32±0.10 and 0.08±0.04 mg  
233 L<sup>-1</sup>, respectively) than at Adj-W (0.26±0.08 and 0.06±0.02 mg L<sup>-1</sup>), respectively. Across stations,  
234 mean POC was highest at BD (0.37±0.10 mg L<sup>-1</sup>), followed by HN (0.32±0.01 mg L<sup>-1</sup>) and NA  
235 (0.24±0.07 mg L<sup>-1</sup>), and lowest at KN (0.19±0.02 mg L<sup>-1</sup>) (Fig. 2B). A similar pattern was  
236 observed for PN, with highest values at BD (0.10 ± 0.03 mg L<sup>-1</sup>), followed by HN (0.07±0.01 mg  
237 L<sup>-1</sup>), NA (0.06±0.00 mg L<sup>-1</sup>), and KN (0.04±0.01 mg L<sup>-1</sup>). The POC/PN ratio ranged from 2.9  
238 (NA\_1500) to 5.4 (NA\_MDS). The POC/PN ratio showed an increasing trend from MDS to Adj-  
239 W for all stations, except NA (Fig. 2C). The NA station showed a decreasing trend in POC/PN  
240 ratio from MDS (5.4) to Adj-W (2.9) with the highest change of 2.5.

241 The δ<sup>13</sup>C and δ<sup>15</sup>N values of POM varied from -26.8‰ (NA\_500) to -29.1‰ (KN\_1500)  
242 and 2.5 (KN\_1500) to 15.9 (BD\_1500), respectively. Mean δ<sup>13</sup>C values of all MDS stations  
243 (-28.0±0.64‰) were similar to that of Adj-W stations (-28.1±0.67‰). However, individually KN  
244 showed a prominent decreasing trend in δ<sup>13</sup>C (-27.1‰ to -29.1‰) and NA showed an increase of  
245 -28.5‰ to -27.5‰ from MDS to Adj-W, while HN and BD values were confined in a narrow  
246 range (-28.0‰ to -28.5‰). For δ<sup>15</sup>N, the overall average at MDS sites was lower (4.5 ± 0.73‰)  
247 compared to Adj-W (6.4 ± 5.02‰). δ<sup>15</sup>N values variations were minor (2.5‰ to 5.6‰) for KN,



248 HN and NA stations, while the observed values for BD\_500 (12.5‰) and BD\_1500 (15.9‰) were  
249 quite high (Fig. 2B).

250



251

252 **Figure 2.** Relationship between Particulate Organic Carbon (POC %) and Particulate Nitrogen  
253 (PN %) relative to C/N ratio contours (A), dual isotope plot of  $\delta^{13}\text{C}$  and  $\delta^{15}\text{N}$  signatures (B) and  
254  $\delta^{13}\text{C}$  Vs C/N ratio in particulate organic matter (C)

255

### 256 3.3 Biochemical and biomolecular composition of POM

#### 257 3.3.1 Concentrations of carbohydrates, proteins, and lipids

258 Particulate carbohydrate (PCHO) and proteins (PPRT) concentrations showed a decreasing trend  
259 from MDS (PCHO: 55.7 to 109.7  $\mu\text{g L}^{-1}$ ; PRT: 56.7 to 145.5  $\mu\text{g L}^{-1}$ ) to Adj-W (PCHO: 46.2 to  
260 84.6  $\mu\text{g L}^{-1}$ ; PPRT: 32.1 to 94.4  $\mu\text{g L}^{-1}$ ) for all stations (Table 2). Unlike PCHO and PPRT,



261 particulate lipids (PLIP) concentrations showed an increasing trend from MDS to Adj-W for NA  
 262 (59.6  $\mu\text{g L}^{-1}$  to 106.7  $\mu\text{g L}^{-1}$ ) and KN (51.6  $\mu\text{g L}^{-1}$  to 70.9  $\mu\text{g L}^{-1}$ ), and a decreasing trend for BD  
 263 (122.7  $\mu\text{g L}^{-1}$  to 83.3  $\mu\text{g L}^{-1}$ ). For HN stations, HN\_500 (118.1  $\mu\text{g L}^{-1}$ ) showed the highest PLIP  
 264 concentrations followed by HN\_MDS (77.8  $\mu\text{g L}^{-1}$ ) and HN\_1500 (47.5  $\mu\text{g L}^{-1}$ ). Among stations,  
 265 BD stations showed the highest average PCHO (90.7  $\mu\text{g L}^{-1}$ ), PPRT (105.4  $\mu\text{g L}^{-1}$ ), and PLIP  
 266 (105.4  $\mu\text{g L}^{-1}$ ) concentrations.

267

268 **Table 2.** Particulate biochemical composition (P-CHO, P-PRT, P-LIP) and Biopolymeric Carbon  
 269 (BPC) concentrations across various sampling stations

Station	P-CHO ( $\mu\text{g L}^{-1}$ )	P-PRT ( $\mu\text{g L}^{-1}$ )	P-LIP ( $\mu\text{g L}^{-1}$ )	BPC-CHO ( $\mu\text{g L}^{-1}$ )	BPC-PRT ( $\mu\text{g L}^{-1}$ )	BPC-LIP ( $\mu\text{g L}^{-1}$ )	BPC (%)	BPC/POC (%)	Labile (%)
NA_MDS	67.7	61.1	59.6	27.1	29.9	44.7	31.7	31.7	17.8
NA_500	54.9	45.5	67.7	22.0	22.3	50.8	45.1	45.1	21.0
NA_1500	46.2	32.1	106.7	18.5	15.7	80.0	60.0	60.0	18.0
BD_MDS	109.7	145.5	122.7	43.9	71.3	92.0	46.3	46.3	25.7
BD_500	84.6	94.4	110.3	33.8	46.3	82.7	40.0	40.0	19.7
BD_1500	77.8	64.2	83.3	31.1	31.5	62.4	47.7	47.7	23.9
KN_MDS	55.7	56.7	51.6	22.3	27.8	38.7	42.2	42.2	23.8
KN_500	46.8	42.6	51.9	18.7	20.9	38.9	46.9	46.9	23.7
KN_1500	53.4	39.1	70.9	21.4	19.2	53.1	50.1	50.1	21.7
HN_MDS	78.6	97.0	77.8	31.4	47.5	58.3	43.4	43.4	25.0
HN_500	75.3	86.2	118.1	30.1	42.2	88.6	49.5	49.5	22.2
HN_1500	73.7	81.8	47.5	29.5	40.1	35.6	33.5	33.5	22.2

270 BPC\_CHO: Biopolymeric carbon equivalent carbohydrate; BPC\_PRT: Carbon equivalent  
 271 biopolymeric protein; BPC\_LIP: Carbon equivalent biopolymeric lipid



272

### 273 *3.3.2 Biopolymeric vs. Non-Biopolymeric Carbon in POM*

274 BPC (%) ranged from 31.7% at NA\_MDS to 60.0% across sampling stations. A consistent increase  
275 from MDS to Adj-W was observed at NA (31.7–60.0%) and KN (42.2–50.1%). In contrast, BD  
276 exhibited lower BPC at BD\_500 (40.0%) compared to both BD\_MDS (46.3%) and BD\_1500  
277 (47.7%) (Table 2). For HN, BPC% was highest at HN\_500 (49.5%) compared to HN\_MDS  
278 (43.4%) and HN\_1500 (33.5%). Overall, BPC\_CHO and BPC\_PPRT, as labile components of  
279 POC, contributed from 17.8% (NA\_MDS) to 25.7% (BD\_MDS) with a difference of 2–6% among  
280 MDS and Adj-W at individual stations. The highest variation was at BD sites with BD\_500  
281 showing the 19.6% of labile components contributions followed by BD\_1500 (23.9%) and  
282 BD\_MDS (25.7%).

283

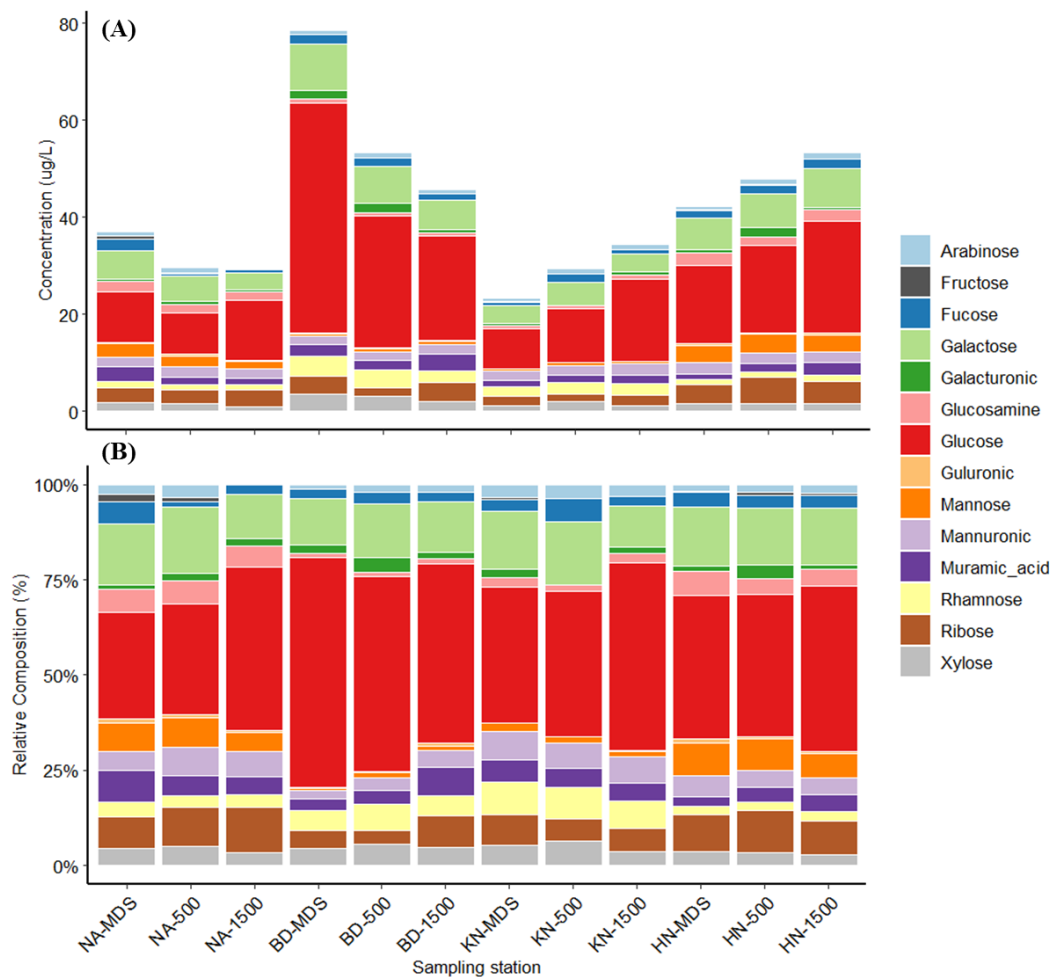
### 284 *3.3.3 Monosaccharide composition of POM*

285 POM monosaccharides comprised glucose, galactose, ribose, rhamnose, fucose, arabinose,  
286 glucosamine, xylose, mannose, fructose, muramic acid, galacturonic acid, guluronic acid (as  
287 mannuronic acid equivalents), and mannuronic acid, with total concentrations highest at BD\_MDS  
288 (78.6  $\mu\text{g L}^{-1}$ ) and lowest at KN\_MDS (23.4  $\mu\text{g L}^{-1}$ ) (Fig. 3A). Total monosaccharide  
289 concentrations at NA and BD declined from MDS to Adj-W, decreasing from 37.0 to 29.3  $\mu\text{g L}^{-1}$   
290 and from 78.6 to 45.6  $\mu\text{g L}^{-1}$ , respectively. In contrast, KN and HN exhibited increasing total  
291 monosaccharide concentrations from MDS to Adj-W, rising from 23.4 to 34.3  $\mu\text{g L}^{-1}$  and from  
292 42.3 to 53.4  $\mu\text{g L}^{-1}$ , respectively. Glucose (8.6 - 47.5  $\mu\text{g L}^{-1}$ ) and galactose (3.4 - 9.6  $\mu\text{g L}^{-1}$ )  
293 dominated the monosaccharide pool and followed trends similar to total monosaccharides from



294 MDS to Adj-W across stations. Station-wise, average monosaccharide concentrations were highest  
295 at BD ( $59.2 \mu\text{g L}^{-1}$ ), followed by HN ( $47.9 \mu\text{g L}^{-1}$ ), NA ( $32.0 \mu\text{g L}^{-1}$ ), and KN ( $29.0 \mu\text{g L}^{-1}$ ).

296 The mol% monosaccharide concentrations showed a consistent pattern across MDS and  
297 Adj-W for each station, with minor differences (Fig. 3B). However, BD and KN stations showed  
298 different composition compared to NA and HN stations, mainly attributed to the contribution of  
299 glucosamine and rhamnose. Glucose, the dominant monosaccharide, exhibited a decreasing mol%  
300 trend from MDS to Adj-W at the BD station, whereas it showed an increasing mol% trend offshore  
301 at the other stations.



302

303 **Figure 3.** Spatial variation in monosaccharide composition of surface POM across fjord stations.

304 (A) Concentrations ( $\mu\text{g L}^{-1}$ ) and (B) relative percentage contributions of individual

305 monosaccharides at macroalgal bed (MDS), 500 m, and 1500 m sites at NA, BD, KN, and HN.

306

### 307 3.3.4 Amino acid composition of POM

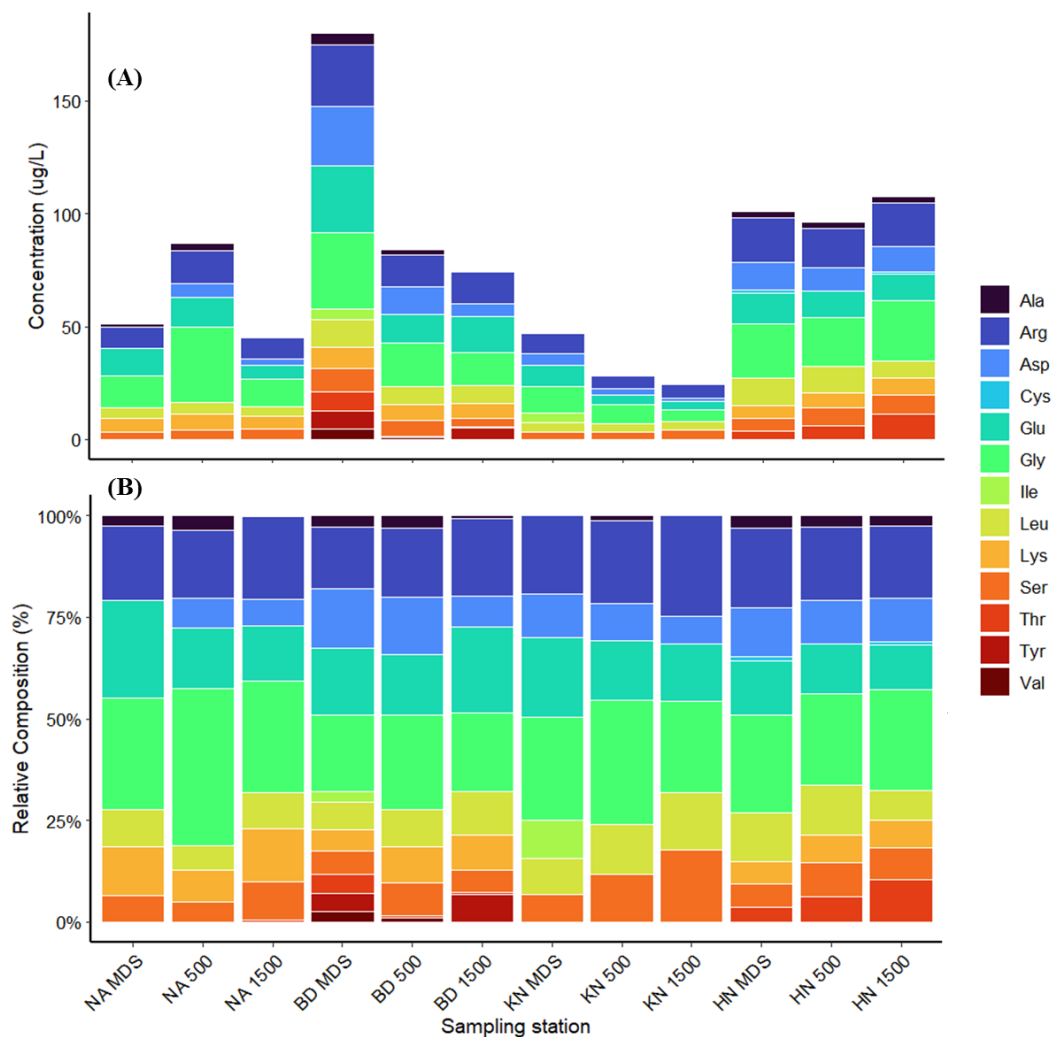
308 Total amino acid concentrations ranged from  $24.4 \mu\text{g L}^{-1}$  (KN\_1500) to  $179.8 \mu\text{g L}^{-1}$  (BD\_MDS).

309 A clear decreasing trend from MDS to Adj-W was observed at BD ( $179.8$  to  $74.8 \mu\text{g L}^{-1}$ ) and KN



310 (47.1 to 24.4  $\mu\text{g L}^{-1}$ ) (Fig. 4A). In contrast, concentrations at NA increased from NA\_MDS (51.2  
311  $\mu\text{g L}^{-1}$ ) to NA\_500 (86.7  $\mu\text{g L}^{-1}$ ) further declined at NA\_1500 (45.1  $\mu\text{g L}^{-1}$ ). At HN, total amino  
312 acid concentrations decreased slightly from HN\_MDS (101  $\mu\text{g L}^{-1}$ ) to HN\_500 (96.1  $\mu\text{g L}^{-1}$ ) and  
313 then increased at HN\_1500 (107.6  $\mu\text{g L}^{-1}$ ). Among stations, average total amino acid  
314 concentrations were highest at BD (113  $\mu\text{g L}^{-1}$ ) followed by HN (101.6  $\mu\text{g L}^{-1}$ ), NA (61  $\mu\text{g L}^{-1}$ )  
315 and KN (33.3  $\mu\text{g L}^{-1}$ ). The BD station showed the highest concentrations of individual amino  
316 acids, with Asp (26.1  $\mu\text{g L}^{-1}$ ), Glu (29.8  $\mu\text{g L}^{-1}$ ), Gly (33.9  $\mu\text{g L}^{-1}$ ), Arg (27.6  $\mu\text{g L}^{-1}$ ), and Lys  
317 (9.4  $\mu\text{g L}^{-1}$ ) peaking at the MDS and declining toward Adj-W (Asp: 5.6  $\mu\text{g L}^{-1}$ ; Glu: 15.9  $\mu\text{g L}^{-1}$ ;  
318 Gly: 14.4  $\mu\text{g L}^{-1}$ ; Arg: 14.4  $\mu\text{g L}^{-1}$ ; Lys: 6.5  $\mu\text{g L}^{-1}$ ). A similar decreasing pattern of the individual  
319 amino acids was observed for the KN station. Exceptions from the low individual amino acid  
320 concentrations at Adj-W (500 and 1500 m locations) included high Gly at NA\_500 (33.5  $\mu\text{g L}^{-1}$ ),  
321 and high Gly (26.7  $\mu\text{g L}^{-1}$ ) and Arg (19.1  $\mu\text{g L}^{-1}$ ) at HN\_1500.

322 Mol% concentration of different amino acids indicated that Gly, Glu, and Arg were the  
323 dominant contributors across all sampling stations (Fig. 4B). The mol% concentration of Glu  
324 showed a decreasing trend from MDS to Adj-W at NA (24.1 % to 13.7%), KN (19.7% to 14.0%)  
325 and HN (13.3% to 10.9%) stations, while BD showed increasing trend (MDS: 16.6%; Adj-W:  
326 21.3%). In contrast, Gly and Arg exhibited similar spatial patterns across stations, with Gly  
327 showing its highest mol% contribution at the 500 m station at NA, BD, and KN, while Arg  
328 displayed a consistent increase from MDS to Adj-W across these stations.



329

330 **Figure 4.** Spatial variation in amino acid composition of surface POM across fjord stations. (A)

331 Concentrations ( $\mu\text{g L}^{-1}$ ) and (B) relative percentage contributions of individual amino acid at

332 macroalgal bed (MDS), 500 m, and 1500 m sites at NA, BD, KN, and HN.

333

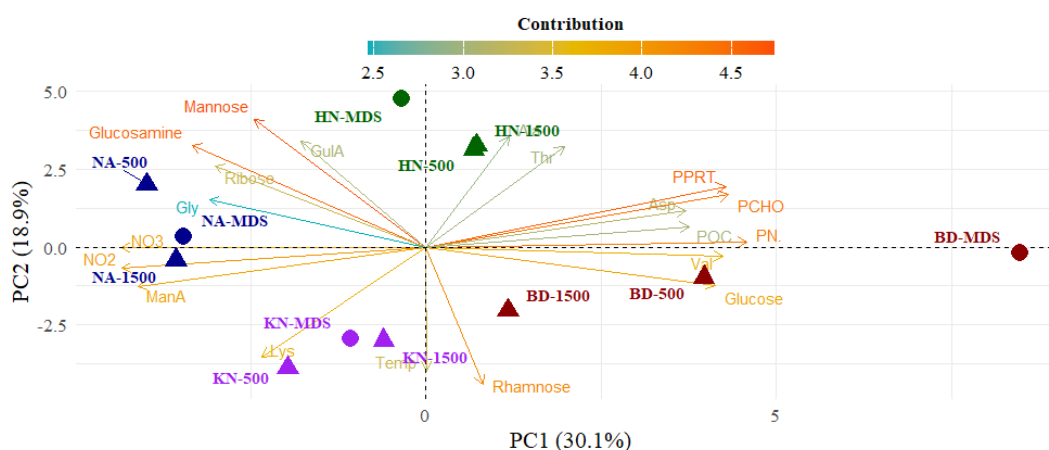
334 **3.4 Statistical analysis**



335 Strong positive correlations were observed between PN with POC, PCHO, and PPRT ( $r > 0.83$ ,  
336  $p < 0.05$ ), with exceptionally high correlation between PPRT and PCHO ( $r = 0.96$ ,  $p < 0.05$ ) (Fig.  
337 S1A). In contrast, the negative correlation was observed between BPC\_LIP% and the non-BPC  
338 fraction ( $r = -0.95$ ,  $p < 0.05$ ), and between nitrate and biochemical parameters (POC, PN, PCHO,  
339 PPRT) ( $r < -0.66$ ,  $p < 0.05$ ). Despite consistent trends across parameters, ANOVA indicated no  
340 significant differences between MDS and Adj-W, suggesting gradual lateral transformations rather  
341 than abrupt distance-related changes, together with pronounced spatial heterogeneity among  
342 stations (Table S1).

343 Mannuronic acid (ManA) showed strong negative correlations with POC ( $r = -0.79$ ) and  
344 P-CHO ( $r = -0.92$ ) (Fig. S1B). Glucose and galactose were negatively correlated with several  
345 compounds, including glucosamine ( $r = -0.72$ ), mannose ( $r = -0.70$ ), ribose ( $r = -0.59$ ), and ManA  
346 ( $r = -0.63$ ). Rhamnose exhibited pronounced negative relationships with guluronic acid (GulA;  $r$   
347  $= -0.83$ ), glucosamine ( $r = -0.76$ ), mannose ( $r = -0.85$ ), and ribose ( $r = -0.73$ ), whereas galactose  
348 was positively correlated with fructose ( $r = 0.61$ ) and arabinose ( $r = 0.58$ ). Strong positive  
349 associations were also observed among mannose, glucosamine ( $r = 0.91$ ), and ribose ( $r = 0.76$ ),  
350 with ribose additionally correlating positively with glucosamine ( $r = 0.79$ ).

351 In PCA analysis, the first two principal components explained 49.0% of the total variance, with  
352 PC1 and PC2 accounting for 30.1% and 18.9%, respectively (Fig. 5). PC1 was positively loaded  
353 by POC, PN, PCHO, PPRT, glucose, galactose, and labile amino acids (Asp, Glu, Thr), whereas  
354 negative PC1 loadings were associated with muramic acid, arabinose, fucose, and inorganic  
355 nutrients. Sample scores showed a spatial organization, with MDS plotting toward positive PC1  
356 values and Adj-W progressively shifting toward negative PC1 values, which was seen more  
357 prominently for BD stations.



358

359 **Figure 5.** Principal Component Analysis (PCA) biplot of biogeochemical variables across  
360 different sample sites. The first two principal components (PC1 and PC2) account for 30.1% and  
361 18.9% of the total variance, respectively. Individual samples are represented by colored shapes,  
362 categorized by site (e.g., NA, HN, KN, BD) and location (e.g., MDS, 500, 1500). Vectors (arrows)  
363 indicate the loadings of specific variables, including carbohydrates (e.g., Mannose, Glucose,  
364 Rhamnose), nutrients ( $\text{NO}_2^-$ ,  $\text{NO}_3^-$ ), and organic matter indicators (POC, PN, PCHO, PPRT). The  
365 color scale of the vectors represents the contribution of each variable to the principal components.

366

#### 367 4. Discussion

##### 368 4.1 Influence of macroalgal beds on surface POM biochemical composition

369 Macroalgal beds produce substantial organic carbon via photosynthesis, which enters into  
370 surrounding waters (Chen et al., 2020; Filbee-Dexter et al., 2022; Pessarrodona et al., 2022;  
371 Watanabe et al., 2020). The observed higher concentrations of POC and PN at MDS relative to  
372 Adj-W, together with consistently higher PCHO and PPRT, indicated localized enrichment of



373 particulate matter near macroalgal beds. The inverse relationship of nitrate with POC, PN, PCHO  
374 and PPRT ( $r = -0.82$ ,  $p < 0.05$ ) reflected biological assimilation of dissolved nutrients into the  
375 particulate pool, reinforcing the role of active coastal production in shaping POM composition  
376 along the fjord gradient. Macroalgal tissues are structurally rich in polysaccharides and contain  
377 substantial protein fractions, and the release of tissue fragments, sloughed material, and epiphyte-  
378 associated biomass (Kennedy and Blain, 2025; Watanabe et al., 2020) which provides a direct  
379 pathway for incorporation of macroalgal carbon into surface POM contributing to Arctic coastal  
380 carbon cycling (Ager et al., 2023). Strong positive correlations ( $r > 0.83$ ,  $p < 0.05$ ) between PN  
381 and POC, PCHO, and PPRT indicate tightly coupled carbon and nitrogen incorporation during  
382 fresh organic matter production. The remarkably strong positive correlation between PPRT and  
383 PCHO ( $r = 0.96$ ,  $p < 0.05$ ) further indicates tightly coupled biological production and POM  
384 synthesis in macroalgal-beds. The multivariate analysis of POM as resolved by PCA showed PC1  
385 (30.1% variance) was dominated by PCHO, PPRT, PN, POC, glucose, and Asp and separated  
386 MDS from Adj-W along a continuous biochemical gradient, especially prominent for BD station  
387 (Fig. 5). The strong positive loadings of labile carbon and nitrogen compounds supported a distinct  
388 organic-rich biochemical state of surface POM at MDS.

389         Although macroalgal biomass and detritus are generally carbon-rich, three of the four  
390 stations (BD, KN, and HN) exhibited lower POC/PN ratios at MDS sites compared to Adj-W. This  
391 pattern likely reflects contributions from fresh, nitrogen-rich organic matter produced within  
392 macroalgal habitats, possibly including phytoplankton, epiphytic microalgae and benthic primary  
393 producers associated with kelp beds (Burfeid-Castellanos et al., 2021; Stanca and Parsons, 2021),  
394 which could be resuspended into surface waters and become part of POM. Kelp forest POM  
395 characteristics are highly variable depending on the water column conditions, which also influence



396 contributions from macroalgal detritus and other autochthonous primary producers (Dyer et al.,  
397 2019). In favorable conditions, other primary producers may possibly outweigh the stoichiometric  
398 signal of macroalgal tissue itself resulting in relatively low POC/PN ratios of POM near  
399 macroalgal beds (Chen et al., 2020). Similarly, heterotrophic bacteria are typically richer in  
400 nitrogen and phosphorus than phytoplankton, and their colonization of particles can lower the bulk  
401 POC/PN ratio by contributing N-rich biomass (Jo et al., 2021). The subsequent increase in  
402 POC/PN ratios from MDS to Adj-W is consistent with preferential microbial degradation of labile  
403 nitrogen-rich compounds during lateral transport (Vidal et al., 2018), leading to relative  
404 enrichment of carbon-rich material with distance from source habitats.

405  $\delta^{13}\text{C}$  values of POM are widely used to trace organic matter sources (Gao et al., 2008;  
406 Pineault et al., 2013). Most macroalgae typically exhibit  $\delta^{13}\text{C}$  values between  $-34.6\text{‰}$  to  $-2.2\text{‰}$   
407 (Velázquez-Ochoa et al., 2022), though some brown macroalgal species show more negative  
408 signatures, ranging from  $-20\text{‰}$  to  $-35\text{‰}$  (Fredriksen, 2003). In Arctic coastal systems, marine  
409 phytoplankton-derived organic matter typically exhibits  $\delta^{13}\text{C}$  values between  $-20$  and  $-26\text{‰}$ ,  
410 whereas terrestrial organic matter derived from C3 vegetation is generally more depleted, around  
411  $-26$  to  $-29\text{‰}$  (Gao et al., 2008; Pineault et al., 2013). However, substantial overlap between  
412 marine and terrestrial isotopic ranges complicates source discrimination in Arctic fjord systems  
413 (Singh et al., 2024b). The similarity of  $\delta^{13}\text{C}$  values between MDS and Adj-W indicated that  
414 macroalgal material does not dominate bulk POM isotopically, but instead contributes  
415 substantially within a mixed particulate pool of macroalgal, phytoplanktonic, and terrestrial  
416 organic matter in Arctic fjords (Ørberg et al., 2023; Roy et al., 2025). This muted isotopic signal  
417 likely reflects that macroalgal influence on surface POM is not solely derived from detached kelp  
418 tissue, but is also mediated by contributions from epiphytic and benthic microalgal production



419 (Burfeid-Castellanos et al., 2021; Stanca and Parsons, 2021) and biochemically distinct macroalgal  
420 fractions, whose  $\delta^{13}\text{C}$  values overlap those of pelagic organic matter.

421  $\delta^{15}\text{N}$  values of POM exceeding  $\sim 2\text{‰}$  as observed in the present study are generally  
422 consistent with marine nitrate-based production and microbial reworking, rather than atmospheric  
423 or  $\text{N}_2$ -fixation sources (Kuzyk et al., 2010), where intense benthic–pelagic coupling and rapid  
424 recycling of dissolved inorganic nitrogen promote isotopic enrichment of the available nitrogen  
425 pool (Elliott Smith and Fox, 2022). Reflecting the pattern more prominently,  $\delta^{15}\text{N}$  value at  
426 BD\_MDS (5.0‰), which was already high, further increased toward Adj-W (BD\_500: 12.5‰,  
427 BD\_1500: 15.9‰), indicating relatively fresher marine-derived organic matter within the  
428 macroalgal beds getting transformed to relatively higher trophic contributions in surrounding  
429 waters.

430

#### 431 **4.2 Transformation of surface POM during lateral transport from macroalgal beds** 432 **to adjacent waters**

433 The biochemical composition of POM provides valuable insights into the nature of organic carbon  
434 and its benthic-pelagic coupling in macroalgal beds (Elliott Smith and Fox, 2022; Renaud et al.,  
435 2015). The observed systematic offshore changes in POM composition revealed both lateral  
436 transport and early transformation of macroalgal-bed derived particles across the fjord (Vidal et  
437 al., 2018). The concentrations of PCHO and PPRT declined consistently from MDS toward Adj-  
438 W, indicating progressive dilution of organic matter sourced from macroalgal-beds, including  
439 shredding's, detritus, associated autochthonous production with distance (Ørberg et al., 2023;  
440 Smale et al., 2022; Simpkins et al., 2025). These labile compounds are preferentially consumed by  
441 particle-associated and free-living microbes (Jain et al., 2019), serving as indicators of freshly



442 produced, easily degradable organic matter (Li et al., 2025). In contrast, PLIP generally increased  
443 offshore (except at BD), indicating a relative enrichment of lipid-rich pelagic material and/or the  
444 preferential preservation of more stable lipid compounds during transport. This pattern likely  
445 reflects selective microbial degradation of labile carbohydrates and proteins during lateral  
446 transport, combined with mixing with newly produced pelagic material (Li et al., 2025),  
447 highlighting dynamic compositional transformation of POM from MDS to Adj-W.

448       The compositional shift in POM was further supported by changes observed in BPC  
449 fractions. BPC represents the relatively labile and bioavailable fraction of POM, mainly  
450 comprising of proteins, carbohydrates, and a lipid fraction, whereas the non-BPC fraction includes  
451 more refractory components such as lignin, humic substances, black carbon, and cellulose  
452 (Fabiano et al., 1993; Lobbes et al., 2000; Tselepidis et al., 2000). Among BPC constituents,  
453 %BPC\_lipid increased markedly from MDS ( $17.8 \pm 2.8\%$ ) to Adj-W ( $25.1 \pm 8.6\%$ ), whereas the  
454 labile fraction (proteins and carbohydrates) showed only minor differences between MDS ( $23.1 \pm$   
455  $3.6\%$ ) and Adj-W ( $21.5 \pm 2.5\%$ ). This pattern suggests a relative enrichment of more stable organic  
456 matter within POC, accompanied by lateral degradation of labile components, consistent with the  
457 observed decline in POC from MDS to Adj-W. Further, the strong inverse relationship between  
458 %BPC\_LIP and the non-BPC fraction ( $r = -0.95$ ,  $p < 0.05$ ) suggested biochemical reorganization  
459 of POM during lateral transport, consistent with selective degradation and compositional  
460 restructuring rather than just uniform bulk loss. In support, PCA also showed a progressive  
461 leftward shift from MDS to Adj-W along PC1 (Fig. 5) demonstrating lateral export of POM from  
462 macroalgal-beds to surrounding waters as a gradient, consistent with progressive dilution and  
463 selective transformation during fjord-scale transport of POM.

464



#### 465 **4.3 Molecular-level evidence for macroalgal imprint and early transformation of POM**

466 Molecular fingerprints based on monosaccharides and amino acids offer direct insight into the  
467 origin, bioavailability, and early diagenetic transformation of organic matter (Grosse et al., 2021;  
468 Jo et al., 2022). Glucose is a common constituent of the macroalgal storage polysaccharide  
469 laminarin, while fucose, galactose, and uronic acids (glucuronic, mannuronic, and guluronic acids)  
470 are key monomers of structural polysaccharides such as alginates and fucans (Singh et al., 2024a).  
471 This carbohydrate pool of macroalgae is bound within structurally complex cell wall polymers that  
472 are relatively resistant to microbial degradation (Kennedy and Blain, 2025). In contrast,  
473 phytoplankton cell walls and extracellular matrices are dominated by cellulose, and species-  
474 specific storage glucans, which are recycled relatively rapidly in surface waters (Biersmith and  
475 Benner, 1998). Glucose and galactose were observed to be the dominant monosaccharides  
476 throughout the samples, reflecting a shared baseline of organic matter likely derived from a  
477 mixture of macroalgal detritus, phytoplankton, and bacterial biomass (Li et al., 2025; Smale et al.,  
478 2022). However, the positive correlation of glucose with POC and PCHO indicated a relative  
479 enrichment of a labile, carbohydrate-rich organic matter pool at MDS where POC and PCHO were  
480 higher than Adj-W. On the other hand, the negative correlation between glucose and other  
481 monosaccharides such as galactose, mannose, mannuronic acid, ribose, and glucosamine reflected  
482 a relative increase in structurally complex, algal, microbial, and zooplankton-associated sugars  
483 during lateral transport and early diagenesis.

484 Amino acid distributions provide the complementary evidence for POM source and lability  
485 patterns, as their composition reflects both the origin and degree of degradation (Grosse et al.,  
486 2021; Jo et al., 2022). The total particulate amino acid concentrations observed in this study (24–  
487 180  $\mu\text{g L}^{-1}$ ) fall within the reported values from coastal Kongsfjorden (Zhu et al., 2016) and across



488 Fram-Strait (Grosse et al., 2021). In this study, the average total amino acids were higher at MDS  
489 ( $94.8 \mu\text{g L}^{-1}$ ) than Adj-W ( $68.4 \mu\text{g L}^{-1}$ ), with BD exhibiting the highest average concentration  
490 ( $113.0 \mu\text{g L}^{-1}$ ), indicating fresher, nitrogen-rich, proteinaceous POM in surface waters along with  
491 elevated PPRT and low C:N ratios observed near macroalgal beds. At BD and KN, total amino  
492 acids drop by ~60–50% from MDS to Adj-W, indicating preferential microbial removal of  
493 proteinaceous, N-rich material during lateral transport, consistent with observed offshore increase  
494 in POC/PN and PLIP enrichment. NA and HN show mid-station or distal increases (NA\_500,  
495 HN\_1500), likely reflect local resuspension or secondary production, supporting spatial  
496 heterogeneity as discussed before. The combined Asp + Glu content, reflecting the freshness of  
497 organic matter and the diagnostic Asp/Gly ratio, indicates the degradation state of organic matter  
498 (Machado et al., 2020; Yao et al., 2023). The decline in Glu, Asp, and Asp/Gly ratio, and relative  
499 enrichment of Gly and Arg from MDS to Adj-W for most of the stations further provide molecular  
500 evidence for early-stage protein degradation and microbial reworking of macroalgal-derived POM  
501 during lateral transport.

502 Together, the coupled behavior of carbohydrates and amino acids demonstrated that  
503 macroalgal beds imprint surface POM with a distinct molecular signature that is progressively  
504 modified during fjord-scale export. These molecular patterns corroborate the bulk biochemical and  
505 isotopic evidence, indicating that macroalgal-derived organic matter is rapidly redistributed across  
506 coastal gradients while undergoing selective early transformation. The pronounced total  
507 monosaccharides and amino acid enrichment at BD (especially BD\_MDS), which also exhibited  
508 the highest POC and PPRT concentrations, identifies this site as a biogeochemical hotspot of  
509 macroalgal influence, reinforcing the spatial coherence of macroalgal signatures across  
510 independent biochemical proxies.



#### 511 **4.4 Brandal (BD) as a biogeochemical hotspot of macroalgal influence in Kongsfjorden**

512 BD station, among all studied stations, consistently emerged as an organic-rich site, showing  
513 characteristics of macroalgal-influenced surface POM, highlighting its role as a biogeochemical  
514 hotspot within Kongsfjorden. With the highest concentrations of POC, PN, PCHO, PPRT, total  
515 monosaccharides, and total amino acids, the BD station contributed maximum in the PCA biplot  
516 (Fig. 5), which demonstrated local production and accumulation of biochemically labile organic  
517 matter within this macroalgal-dominated habitat. The strong gradient observed across PN,  $\delta^{15}\text{N}$ ,  
518 C:N, PPRT, and amino acid composition from MDS to Adj-W at BD, indicated nitrogen  
519 assimilation, dominance of fresh marine organic matter in macroalgal bed and their progressive  
520 downstream alteration. At the molecular level also, BD\_MDS was strongly enriched in glucose  
521 and other macroalgal sugars (fucose, galactose, mannuronic acid), with total monosaccharides and  
522 glucose declining offshore. Similarly, the offshore decrease in labile amino acids (e.g., Asp, Glu)  
523 provides molecular evidence for early degradation during export, indicating that the BD  
524 macroalgal bed is a major source of biochemically active POM and a key contributor to fjord-scale  
525 redistribution.

526 Situated on the westernmost part of the south shore, BD is influenced by Atlantic water  
527 inflow, resulting in relatively warmer and more saline conditions (Williams et al., 2017) and  
528 supports abundant microphytobenthos, as well as benthic mosses that contribute significantly to  
529 primary production, stabilize sediments, and sustain diverse benthic food webs (Woelfel et al.,  
530 2014). The BD site is characterized by high macroalgal detrital cover and meiofaunal density in  
531 Kongsfjorden (Schimani et al., 2022). Shallow habitats further support diverse fish and  
532 invertebrate assemblages, often associated with macroalgal beds that offer both food and shelter  
533 (Wilson et al., 2022). Collectively, these features make BD an optimal site for the deposition and

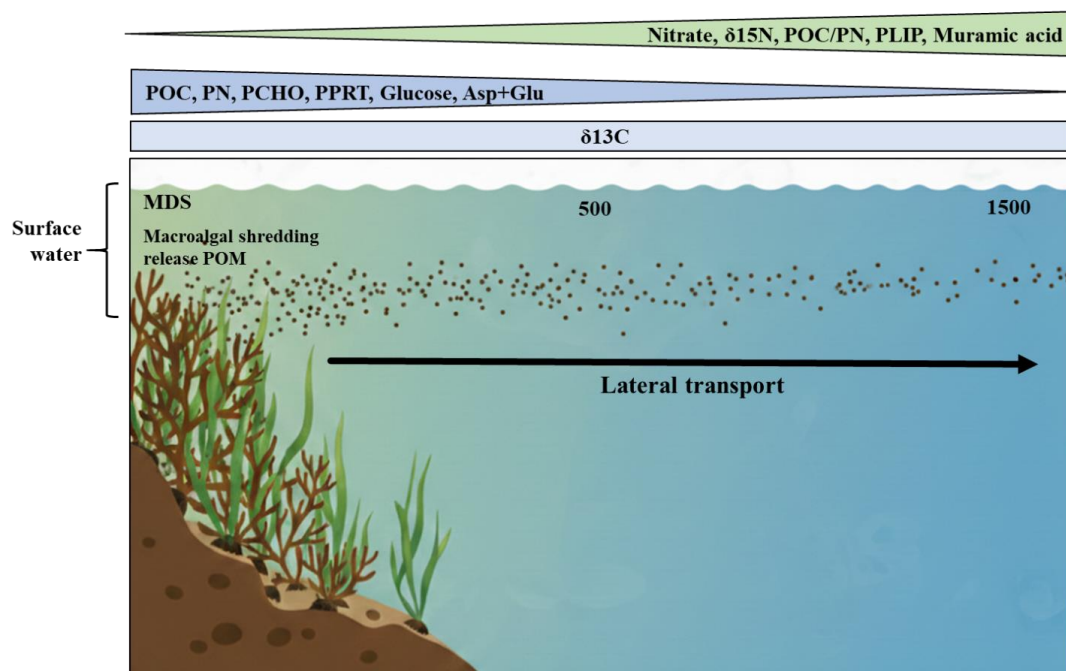


534 retention of macroalgal detritus, contributing to the exceptionally high concentrations of labile and  
535 refractory organic matter as observed in both particulate and biopolymeric pools in this study.

536

#### 537 **4.5 Implications of macroalgal-beds for Arctic coastal carbon cycling**

538 The present study provided a multi-proxy assessment of POM in surface waters of macroalgal beds  
539 in Kongsfjorden, integrating bulk biogeochemistry, isotopes, biopolymeric composition, and  
540 molecular biomarkers. Elevated bulk (POC, PN, PCHO, and PPRT) and molecular  
541 (monosaccharides and amino acids) concentrations at macroalgal-dominated sites indicated that  
542 macroalgal beds act as localized sources of biochemically labile organic matter. The results  
543 demonstrated that macroalgal beds imprint surface waters with distinct biochemical and molecular  
544 signatures that are rapidly redistributed across fjord-scale gradients. The PCA demonstrates that  
545 macroalgal influence structures surface POM along a continuous multivariate gradient rather than  
546 discrete habitat classes. The systematic offshore decline of these compounds, together with internal  
547 reorganization of biopolymeric and molecular composition, shows that macroalgal-derived POM  
548 is efficiently exported and selectively transformed during lateral transport (Fig. 6).



549

550 **Figure 6.** Schematic showing biochemical nature of POM at macroalgal-dominated sites and its  
551 transformation during lateral transport

552 The modest changes in bulk isotopic composition and overall POM lability indicate that  
553 macroalgal influence is expressed not as simple replacement of pelagic organic matter, but through  
554 continuous mixing and biochemical restructuring of a heterogeneous particulate pool. Macroalgal-  
555 beds influenced by carbon can enter surface waters both directly, via tissue erosion, and indirectly,  
556 via stimulation of associated epiphytic and primary production, highlighting the complexity of  
557 benthic–pelagic coupling in Arctic coastal systems. Our study demonstrates that macroalgal-  
558 dominated sites in Kongsfjorden act as hotspots of labile and bioavailable organic matter,  
559 significantly shaping the composition and lability of POM in adjacent waters. The intermediate  
560 and variable patterns observed at the few stations highlight that the influence of MDS was not  
561 uniform but forms a gradient shaped by local hydrodynamics, freshwater inputs, and nutrient



562 availability. The strong spatial heterogeneity observed, particularly the emergence of Brandal as a  
563 biogeochemical hotspot, emphasizes that macroalgal impacts on coastal carbon cycling are  
564 unevenly distributed within fjord systems. Such localized but persistent sources of organic carbon  
565 from macroalgal-beds to surrounding waters and thereby dampening seasonal variability in carbon  
566 availability (Norkko et al., 2007), enhancing benthic-pelagic food-web stability and increase  
567 ecosystem resilience to interannual fluctuations in pelagic primary production (Norkko et al.,  
568 2007; Renaud et al., 2015).

569         Although our study focused on surface waters, future research should include vertical  
570 fluxes of POM near macroalgal beds and their coupling to hydrodynamics. Additionally, effects  
571 of seasonal variability driven by glacial melt, riverine runoff, and episodic nutrient inputs at coast  
572 are important as they can alter carbon concentrations and biochemical composition, particularly in  
573 nearshore macroalgal habitats (Ager et al., 2023). Experimental studies at model sites like BD  
574 could further help in elucidating the rates of labile carbon turnover, microbial utilization, and  
575 nutrient remineralization at these sites. As macroalgal habitats are expanding under ongoing  
576 warming, resolving the contribution of macroalgal biomass and beds-associated organic matter  
577 dynamics in coastal biogeochemistry would be important for estimating Arctic carbon budgets and  
578 ecosystem functioning.

579

## 580 **Conclusion**

581 The present study provides new insights into the role of Arctic macroalgal beds as active drivers  
582 of coastal particulate organic matter dynamics in Kongsfjorden, an Arctic fjord. By integrating  
583 bulk biogeochemical properties, stable isotopes, biopolymeric composition, and molecular  
584 biomarkers, we demonstrate that macroalgal habitats imprint surface waters with a distinct



585 biochemical and molecular signature. Elevated concentrations of POC, PN, carbohydrates,  
586 proteins, monosaccharides, and amino acids at macroalgal-dominated sites indicate that  
587 macroalgal beds act as localized sources of biochemically labile organic matter to the overlying  
588 water column. Systematic offshore declines in bulk parameters, together with internal  
589 reorganization of biopolymeric and molecular composition, reveal that macroalgal-beds derived  
590 POM is efficiently exported across fjord-scale gradients and undergoes selective early-stage  
591 transformation during lateral transport. The muted bulk isotopic gradients further indicate that  
592 macroalgal influence is expressed through continuous mixing and biochemical restructuring of a  
593 heterogeneous particulate pool rather than simple replacement of pelagic organic matter. A  
594 pronounced spatial gradient was observed across the stations, and within which Brandal emerged  
595 as a distinct biogeochemical hotspot of macroalgal-associated organic matter dynamics as evident  
596 from our multiproxy study. Overall, our findings show that macroalgal beds function as dynamic  
597 benthic–pelagic coupling zones that redistribute and transform organic carbon beyond their  
598 immediate habitat. As macroalgal cover continues to expand along Arctic coastlines under climate  
599 warming, their contribution to coastal carbon fluxes is likely to intensify, with important  
600 implications for Arctic carbon budgets and ecosystem functioning.

601

602 **Data availability.** The data is available at Zenodo repository:  
603 <https://doi.org/10.5281/zenodo.18457176> (Jagtap et al., 2026).

604

605 **Author contributions.** ASJ and AS conceptualized the study with input from AJ. AS and AJ  
606 conducted the fieldwork, while laboratory analyses were performed by ASJ and NR. MT analyzed



607 the elemental and isotopic data. All authors were involved in the interpretation of the results, the  
608 revision, and the writing of the final version of the paper.

609

610 **Competing interests.** The contact author has declared that none of the authors has any competing  
611 interests.

612

613 **Acknowledgement.** We extend our gratitude to the Director of the National Centre for Polar and  
614 Ocean Research for their support in this work. We acknowledge funding from the Ministry of  
615 Earth Sciences. We are thankful to Dr. Biswajit Roy, Dr. PV Bhaskar and Ms. Viola Rodrigues  
616 for sampling assistance, nutrient and EA-IRMS analysis, respectively.

617

618 **Financial support.** This research was funded by the National Centre for Polar and Ocean Research  
619 (NCPOR), Ministry of Earth Sciences (MoES), India.

620

## 621 **References**

622 Ager, T. G., Krause-Jensen, D., Olesen, B., Carlson, D. F., Winding, M. H. S., and Sejr, M. K.:  
623 Macroalgal habitats support a sustained flux of floating biomass but limited carbon export  
624 beyond a Greenland fjord, *Sci. Total Environ.*, 872, 162224,  
625 <https://doi.org/10.1016/j.scitotenv.2023.162224>, 2023.

626 Assis, J., Serrão, E. A., Duarte, C. M., Fragkopoulou, E., and Krause-Jensen, D.: Major  
627 Expansion of Marine Forests in a Warmer Arctic, *Front. Mar. Sci.*, 9, 1–10,  
628 <https://doi.org/10.3389/fmars.2022.850368>, 2022.

629 Biersmith, A. and Benner, R.: Carbohydrates in phytoplankton and freshly produced dissolved  
630 organic matter, *Mar. Chem.*, 63, 131–144, [https://doi.org/10.1016/S0304-4203\(98\)00057-7](https://doi.org/10.1016/S0304-4203(98)00057-7),  
631 1998.



- 632 Buchholz, C. M. and Wiencke, C.: Working on a baseline for the Kongsfjorden food web:  
633 production and properties of macroalgal particulate organic matter (POM), *Polar Biol.*, 39, 2053–  
634 2064, <https://doi.org/10.1007/s00300-015-1828-3>, 2016.
- 635 Burfeid-Castellanos, A. M., Martín-Martín, R. P., Kloster, M., Angulo-Preckler, C., Avila, C.,  
636 and Beszteri, B.: Epiphytic diatom community structure and richness is determined by  
637 macroalgal host and location in the South Shetland Islands (Antarctica), *PLoS One*, 16, 1–21,  
638 <https://doi.org/10.1371/journal.pone.0250629>, 2021.
- 639 Carlson, D. F., Suzuki, N., Carrasco, R., Filbee-Dexter, K., Gillard, L. C., Myers, P. G., Queirós,  
640 A. M., Assis, J., Duarte, C. M., Sejr, M., and Krause-Jensen, D.: Ocean transport and vertical  
641 mixing connect Greenland’s macroalgae to deep ocean carbon sinks, *Sci. Total Environ.*, 1012,  
642 <https://doi.org/10.1016/j.scitotenv.2025.181247>, 2026.
- 643 Castro de la Guardia, L., Bartsch, I., Hop, H., Niedzwiedz, S., Düsedau, L., Diehl, N., Krause-  
644 Jensen, D., Sejr, M., Ager, T. G., Gattuso, J. P., Schlegel, R. W., Miller, C. A., Filbee-Dexter, K.,  
645 and Duarte, P.: Predicting potential Arctic kelp distribution and lower-depth biomass from  
646 seafloor irradiance, *Limnol. Oceanogr. Methods*, <https://doi.org/10.1002/lom3.70018>, 2025.
- 647 Chen, S., Xu, K., Ji, D., Wang, W., Xu, Y., Chen, C., and Xie, C.: Release of dissolved and  
648 particulate organic matter by marine macroalgae and its biogeochemical implications, *Algal*  
649 *Res.*, 52, 102096, <https://doi.org/10.1016/j.algal.2020.102096>, 2020.
- 650 Dai, A., Luo, D., Song, M., and Liu, J.: Arctic amplification is caused by sea-ice loss under  
651 increasing CO<sub>2</sub>, *Nat. Commun.*, 10, 1–13, <https://doi.org/10.1038/s41467-018-07954-9>, 2019.
- 652 Danovaro, R., Dell’Anno, A., and Fabiano, M.: Bioavailability of organic matter in the  
653 sediments of the Porcupine Abyssal Plain, northeastern Atlantic, *Mar. Ecol. Prog. Ser.*, 220, 25–  
654 32, <https://doi.org/10.3354/meps220025>, 2001.
- 655 Duarte, C. M., Losada, I. J., Hendriks, I. E., Mazarrasa, I., and Marbà, N.: The role of coastal  
656 plant communities for climate change mitigation and adaptation, *Nat. Clim. Chang.*, 3, 961–968,  
657 <https://doi.org/10.1038/nclimate1970>, 2013.
- 658 Dubois, M., Gilles, K. A., Hamilton, J. K., Rebers, P. A., and Smith, F.: Colorimetric Method for  
659 Determination of Sugars and Related Substances, 350–356, <https://doi.org/10.1021/ac60111a017>,  
660 1956.
- 661 Düsedau, L., Fredriksen, S., Brand, M., Fischer, P., Karsten, U., Bischof, K., Savoie, A., and  
662 Bartsch, I.: Kelp forest community structure and demography in Kongsfjorden (Svalbard) across  
663 25 years of Arctic warming, *Ecol. Evol.*, 14, 1–25, <https://doi.org/10.1002/ece3.11606>, 2024.
- 664 Dyer, D. C., Butler, M. J., Smit, A. J., Anderson, R. J., and Bolton, J. J.: Kelp forest POM during  
665 upwelling and downwelling conditions: Using stable isotopes to differentiate between detritus  
666 and phytoplankton, *Mar. Ecol. Prog. Ser.*, 619, 17–34, <https://doi.org/10.3354/meps12941>, 2019.



- 667 Elliott Smith, E. A. and Fox, M. D.: Characterizing energy flow in kelp forest food webs: a  
668 geochemical review and call for additional research, *Ecography (Cop.)*, 2022, 1–16,  
669 <https://doi.org/10.1111/ecog.05566>, 2022.
- 670 Fabiano, M., Povero, P., and Danovaro, R.: Distribution and composition of particulate organic  
671 matter in the Ross Sea (Antarctica), *Polar Biol.*, 13, 525–533,  
672 <https://doi.org/10.1007/BF00236394>, 1993.
- 673 Filbee-Dexter, K. and Wernberg, T.: Substantial blue carbon in overlooked Australian kelp  
674 forests, *Sci. Rep.*, 10, 1–6, <https://doi.org/10.1038/s41598-020-69258-7>, 2020.
- 675 Filbee-Dexter, K., MacGregor, K. A., Lavoie, C., Garrido, I., Goldsmit, J., Castro de la Guardia,  
676 L., Howland, K. L., Johnson, L. E., Konar, B., McKindsey, C. W., Mundy, C. J., Schlegel, R.  
677 W., and Archambault, P.: Sea Ice and Substratum Shape Extensive Kelp Forests in the Canadian  
678 Arctic, *Front. Mar. Sci.*, 9, 1–27, <https://doi.org/10.3389/fmars.2022.754074>, 2022.
- 679 FOLCH, J., LEES, M., and SLOANE STANLEY, G. H.: A simple method for the isolation and  
680 purification of total lipides from animal tissues., *J. Biol. Chem.*, 226, 497–509,  
681 [https://doi.org/10.1016/s0021-9258\(18\)64849-5](https://doi.org/10.1016/s0021-9258(18)64849-5), 1957.
- 682 Fredriksen, S.: Food web studies in a Norwegian kelp forest based on stable isotope ( $\delta^{13}\text{C}$  and  
683  $\delta^{15}\text{N}$ ) analysis, *Mar. Ecol. Prog. Ser.*, 260, 71–81, <https://doi.org/10.3354/meps260071>, 2003.
- 684 Gao, J., Wang, Y., Pan, S., Zhang, R., Li, J., and Bai, F.: Spatial distributions of organic carbon  
685 and nitrogen and their isotopic compositions in sediments of the Changjiang Estuary and its  
686 adjacent sea area, *J. Geogr. Sci.*, 18, 46–58, <https://doi.org/10.1007/s11442-008-0046-0>, 2008.
- 687 Grasshoff: *Methods\_Seawater\_Analysis*, 2009.
- 688 Grosse, J., Nöthig, E. M., Torres-Valdés, S., and Engel, A.: Summertime Amino Acid and  
689 Carbohydrate Patterns in Particulate and Dissolved Organic Carbon Across Fram Strait, *Front.*  
690 *Mar. Sci.*, 8, <https://doi.org/10.3389/fmars.2021.684675>, 2021.
- 691 Jagtap, A., Singh, A., jain, . anand ., Tiwari, M., and Raj, N.: Particulate Organic Matter  
692 composition in and around macroalgal beds in Kongsfjorden, Arctic, Zenodo,  
693 <https://doi.org/https://doi.org/10.5281/zenodo.18457176>, 2026.
- 694 Jain, A., Krishnan, K. P., Singh, A., Thomas, F. A., Begum, N., Tiwari, M., Bhaskar, V. P., and  
695 Gopinath, A.: Biochemical composition of particles shape particle-attached bacterial community  
696 structure in a high Arctic fjord, *Ecol. Indic.*, 102, 581–592,  
697 <https://doi.org/10.1016/j.ecolind.2019.03.015>, 2019.
- 698 Jo, N., La, H. S., Kim, J. H., Kim, K., Kim, B. K., Kim, M. J., Son, W., and Lee, S. H.: Different  
699 Biochemical Compositions of Particulate Organic Matter Driven by Major Phytoplankton  
700 Communities in the Northwestern Ross Sea, *Front. Microbiol.*, 12,  
701 <https://doi.org/10.3389/fmicb.2021.623600>, 2021.



- 702 Jo, N., Youn, S. H., Joo, H. T., Jang, H. K., Kim, Y., Park, S., Kim, J., Kim, K., Kang, J. J., and  
703 Lee, S. H.: Seasonal variations in biochemical (biomolecular and amino acid) compositions and  
704 protein quality of particulate organic matter in the Southwestern East/Japan Sea, *Front. Mar. Sci.*,  
705 9, <https://doi.org/10.3389/fmars.2022.979137>, 2022.
- 706 Karl Attard; Rakesh Kumar Singh, J.-P., Gattusof, Karen Filbee-Dexter, Dorte Krause-Jensen,  
707 M. K., and Mikael K. Sejr, Philippe Archambault, Marcel Babin, Simon Bélanger, Peter Berg,  
708 Ronnie N. Glud, Kasper Hancke, Stefan Jänicke, Jing Qin, Søren Rysgaard, Esben B. Sørensen,  
709 Foucaut Tachon, Frank Wenzhöfer, and M. A.: Seafloor primary production in a changing  
710 Arctic Ocean, *PNAS*, 121, e2303366121, 2024.
- 711 Kennedy, J. R. and Blain, C. O.: A systematic review of marine macroalgal degradation: Toward  
712 a better understanding of macroalgal carbon sequestration potential, *J. Phycol.*, 61, 399–432,  
713 <https://doi.org/10.1111/jpy.70031>, 2025.
- 714 Kim, J., Jo, N., Park, J., Kim, K., Park, S., Kim, Y., Kim, J., Kim, B. K., Lee, B., and Lee, S. H.:  
715 Different amino acid compositions and food quality of particulate organic matter driven by two  
716 major phytoplankton groups in the Ross Sea, *J. Sea Res.*, 201, 102524,  
717 <https://doi.org/10.1016/j.seares.2024.102524>, 2024.
- 718 Krause-Jensen, D. and Duarte, C. M.: Substantial role of macroalgae in marine carbon  
719 sequestration, *Nat. Geosci.*, 9, 737–742, <https://doi.org/10.1038/ngeo2790>, 2016.
- 720 Krause-Jensen, D., Archambault, P., Assis, J., Bartsch, I., Bischof, K., Filbee-Dexter, K.,  
721 Dunton, K. H., Maximova, O., Ragnarsdóttir, S. B., Sejr, M. K., Simakova, U., Spiridonov, V.,  
722 Wegeberg, S., Winding, M. H. S., and Duarte, C. M.: Imprint of Climate Change on Pan-Arctic  
723 Marine Vegetation, *Front. Mar. Sci.*, 7, 1–28, <https://doi.org/10.3389/fmars.2020.617324>, 2020.
- 724 Kuzyk, Z. Z. A., Macdonald, R. W., Tremblay, J. É., and Stern, G. A.: Elemental and stable  
725 isotopic constraints on river influence and patterns of nitrogen cycling and biological  
726 productivity in Hudson Bay, *Cont. Shelf Res.*, 30, 163–176,  
727 <https://doi.org/10.1016/j.csr.2009.10.014>, 2010.
- 728 Li, H., Zhang, Z., Chen, J., Nair, S., Xiong, T., Zhao, H., He, D., Lee, K., Jiao, N., and Zhang,  
729 Y.: Fate and carbon sequestration potential of sunken macroalgae in coastal oceans from long-  
730 term microbial degradation perspective, *Natl. Sci. Rev.*, 12, <https://doi.org/10.1093/nsr/nwaf273>,  
731 2025.
- 732 Lobbes, J. M., Fitznar, H. P., and Kattner, G.: Biogeochemical characteristics of dissolved and  
733 particulate organic matter, *Geochim. Cosmochim. Acta*, 64, 2973–2983, 2000.
- 734 Machado, M., Machado, S., Pimentel, F. B., Freitas, V., Alves, R. C., and Oliveira, M. B. P. P.:  
735 Amino acid profile and protein quality assessment of macroalgae produced in an integrated  
736 multi-trophic aquaculture system, *Foods*, 9, <https://doi.org/10.3390/foods9101382>, 2020.



- 737 Mathew, S., Hong, J. K., Kim, J. H., Chen, M., and Hur, J.: Terrestrial inputs of nutrients and  
738 dissolved organic carbon to the Arctic Ocean and their influence on primary production, *Mar.*  
739 *Environ. Res.*, 209, 107182, <https://doi.org/10.1016/j.marenvres.2025.107182>, 2025.
- 740 McGovern, M., Pavlov, A. K., Deininger, A., Granskog, M. A., Leu, E., Søreide, J. E., and Poste,  
741 A. E.: Terrestrial Inputs Drive Seasonality in Organic Matter and Nutrient Biogeochemistry in a  
742 High Arctic Fjord System (Isfjorden, Svalbard), *Front. Mar. Sci.*, 7, 1–15,  
743 <https://doi.org/10.3389/fmars.2020.542563>, 2020.
- 744 van der Mheen, M., Wernberg, T., Pattiaratchi, C., Pessarrodona, A., Janekovic, I., Simpkins, T.,  
745 Hovey, R., and Filbee-Dexter, K.: Substantial kelp detritus exported beyond the continental shelf  
746 by dense shelf water transport, *Sci. Rep.*, 14, 1–12, <https://doi.org/10.1038/s41598-023-51003-5>,  
747 2024.
- 748 Niedzwiedz, S., Voigt, C., Andersen, S., Diehl, N., Descôteaux, R., Damsgård, B., and Bischof,  
749 K.: Biochemistry of Arctic kelp specimens is conditioned by the local environment, *Mar.*  
750 *Environ. Res.*, 212, <https://doi.org/10.1016/j.marenvres.2025.107604>, 2025.
- 751 Norkko, A., Thrush, S. F., Cummings, V. J., Gibbs, M. M., Andrew, N. L., Norkko, J., and  
752 Schwarz, A. M.: Trophic structure of coastal Antarctic food webs associated with changes in sea  
753 ice and food supply, *Ecology*, 88, 2810–2820, <https://doi.org/10.1890/06-1396.1>, 2007.
- 754 Ørberg, S. B., Duarte, C. M., Geraldi, N. R., Sejr, M. K., Wegeberg, S., Hansen, J. L. S., and  
755 Krause-Jensen, D.: Prevalent fingerprint of marine macroalgae in arctic surface sediments, *Sci.*  
756 *Total Environ.*, 898, <https://doi.org/10.1016/j.scitotenv.2023.165507>, 2023.
- 757 Ortega, A., Geraldi, N. R., Alam, I., Kamau, A. A., Acinas, S. G., Logares, R., Gasol, J. M.,  
758 Massana, R., Krause-Jensen, D., and Duarte, C. M.: Important contribution of macroalgae to  
759 oceanic carbon sequestration, *Nat. Geosci.*, 12, 748–754, <https://doi.org/10.1038/s41561-019-0421-8>, 2019.
- 761 Pedersen, M. F., Filbee-Dexter, K., Frisk, N. L., Sárossy, Z., and Wernberg, T.: Carbon  
762 sequestration potential increased by incomplete anaerobic decomposition of kelp detritus, *Mar.*  
763 *Ecol. Prog. Ser.*, 660, 53–67, <https://doi.org/10.3354/meps13613>, 2021.
- 764 Pessarrodona, A., Assis, J., Filbee-Dexter, K., Burrows, M. T., Gattuso, J. P., Duarte, C. M.,  
765 Krause-Jensen, D., Moore, P. J., Smale, D. A., and Wernberg, T.: Global seaweed productivity,  
766 *Sci. Adv.*, 8, <https://doi.org/10.1126/sciadv.abn2465>, 2022.
- 767 Pineault, S., Tremblay, J. É., Gosselin, M., Thomas, H., and Shadwick, E.: The isotopic signature  
768 of particulate organic C and N in bottom ice: Key influencing factors and applications for tracing  
769 the fate of ice-algae in the Arctic Ocean, *J. Geophys. Res. Ocean.*, 118, 287–300,  
770 <https://doi.org/10.1029/2012JC008331>, 2013.
- 771 Rantanen, M., Karpechko, A. Y., Lipponen, A., Nordling, K., Hyvärinen, O., Ruosteenoja, K.,  
772 Vihma, T., and Laaksonen, A.: The Arctic has warmed nearly four times faster than the globe



- 773 since 1979, *Commun. Earth Environ.*, 3, 1–10, <https://doi.org/10.1038/s43247-022-00498-3>,  
774 2022.
- 775 Renaud, P. E., Løkken, T. S., Jørgensen, L. L., Berge, J., and Johnson, B. J.: Macroalgal detritus  
776 and food-web subsidies along an Arctic fjord depth-gradient, *Front. Mar. Sci.*, 2, 1–15,  
777 <https://doi.org/10.3389/fmars.2015.00031>, 2015.
- 778 Roy, B., Singh, A., and Tiwari, M.: Tracing macroalgal-induced changes in carbon dynamics of  
779 high-Arctic fjords using biomarker fingerprinting. *J. Geophys. Res. Oceans*, 130(4),  
780 e2024JC021900, <https://doi.org/10.1029/2024JC021900>, 2025.
- 781 Schimani, K., Zacher, K., Jerosch, K., Pehlke, H., Wiencke, C., and Bartsch, I.: Video survey of  
782 deep benthic macroalgae and macroalgal detritus along a glacial Arctic fjord: Kongsfjorden  
783 (Spitsbergen), *Polar Biol.*, 45, 1291–1305, <https://doi.org/10.1007/s00300-022-03072-x>, 2022.
- 784 Singh, A., Pal, B., and Singh, K. S.: Carbohydrate and pigment composition of macroalgae in a  
785 kelp-dominated Arctic fjord, *Reg. Stud. Mar. Sci.*, 77, 103644,  
786 <https://doi.org/10.1016/j.rsma.2024.103644>, 2024a.
- 787 Singh, A., Jain, A., Singh, R., Singh, K. S., Roy, B., Tiwari, M., David T., D., and Jagtap, A.:  
788 Tracing marine and terrestrial biochemical signatures of particulate organic matter in an Arctic  
789 fjord (Kongsfjorden), *Mar. Chem.*, 267, 104468,  
790 <https://doi.org/10.1016/j.marchem.2024.104468>, 2024b.
- 791 Smale, D. A., Pessarrodona, A., King, N., and Moore, P. J.: Examining the production, export,  
792 and immediate fate of kelp detritus on open-coast subtidal reefs in the Northeast Atlantic,  
793 *Limnol. Oceanogr.*, 67, S36–S49, <https://doi.org/10.1002/lno.11970>, 2022.
- 794 Stanca, E. and Parsons, M. L.: Examining the dynamic nature of epiphytic microalgae in the  
795 Florida Keys: What factors influence community composition?, *J. Exp. Mar. Bio. Ecol.*, 538,  
796 <https://doi.org/10.1016/j.jembe.2021.151538>, 2021.
- 797 Taylor Simpkins, Mirjam Van Der Mheen, Morten F. Pedersen, A. P. and Chari Pattiaratchi,  
798 Thomas Wernberg, K. F.-D.: Macroalgae detritus decomposition and cross-shelf carbon export  
799 from shallow and deep reefs, <https://doi.org/10.1002/lno.70006>, 2025.
- 800 Tselepides, A., Polychronaki, T., Marrale, D., Akoumianaki, I., Dell'Anno, A., Pusceddu, A.,  
801 and Danovaro, R.: Organic matter composition of the continental shelf and bathyal sediments of  
802 the Cretan Sea (NE Mediterranean), *Prog. Oceanogr.*, 46, 311–344,  
803 [https://doi.org/10.1016/S0079-6611\(00\)00024-0](https://doi.org/10.1016/S0079-6611(00)00024-0), 2000.
- 804 Upreti, G. C., Ratcliff, R. A., and Riches, P. C.: Protein Estimation in Tissues Containing High  
805 Levels of Lipid : Modifications to Lowry ' s Method of Protein Determination Effect of  
806 Detergents upon NADPH- Generating Enzymes Protein Estimation by the BCA Method, 427,  
807 421–427, [https://doi.org/10.1016/0003-2697\(88\)90339-9](https://doi.org/10.1016/0003-2697(88)90339-9) 1988.



- 808 Velázquez-Ochoa, R., Ochoa-Izaguirre, M. J., and Soto-Jiménez, M. F.: An analysis of the  
809 variability in  $\delta^{13}\text{C}$  in macroalgae from the Gulf of California: Indicative of carbon concentration  
810 mechanisms and isotope discrimination during carbon assimilation, *Biogeosciences*, 19, 1–27,  
811 <https://doi.org/10.5194/bg-19-1-2022>, 2022.
- 812 Vidal, M., Aspillaga, E., Teixidor-Toneu, I., & Delgado-Huertas, A.: Lateral Transport of N-rich  
813 dissolved organic matter strengthens phosphorus deficiency in western subtropical North Atlantic.  
814 *Global Biogeochem. Cy.* 32(9), 1350–1366, <https://doi.org/10.1029/2017GB005868>, 2018.
- 815 Watanabe, K., Yoshida, G., Hori, M., Umezawa, Y., Moki, H., and Kuwae, T.: Macroalgal  
816 metabolism and lateral carbon flows create extended atmospheric  $\text{CO}_2$  sinks, *Biogeosciences*  
817 *Discuss.*, 1–25, <https://doi.org/10.5194/bg-17-2425-2020>, 2020.
- 818 Williams, L., Borchhardt, N., Colesie, C. et al.: Biological soil crusts of Arctic Svalbard and of  
819 Livingston Island, Antarctica. *Polar Biol.* 40, 399–411. [https://doi.org/10.1007/s00300-016-1967-](https://doi.org/10.1007/s00300-016-1967-1)  
820 1, 2017.
- 821 Wilson, S. K., Fulton, C. J., Graham, N. A., Abesamis, R., Berkström, C., Coker, D. J., et al.:  
822 The contribution of macroalgae-associated fishes to small-scale tropical reef fisheries. *Fish Fish.*  
823 23(4), 847–861, <https://doi.org/10.1111/faf.12653>, 2022.
- 824 Woelfel, J., Eggert, A., and Karsten, U.: Marginal impacts of rising temperature on Arctic  
825 benthic microalgae production based on in situ measurements and modelled estimates, *Mar.*  
826 *Ecol. Prog. Ser.*, 501, 25–40, <https://doi.org/10.3354/meps10688>, 2014.
- 827 Yao, X., Fan, T., Gao, G., Liu, L., Chao, J., and Liu, H.: Spatiotemporal pattern and  
828 biodegradation process of amino acids in the large shallow eutrophic lake Taihu, China, *Environ.*  
829 *Sci. Pollut. Res.*, 30, 12584–12595, <https://doi.org/10.1007/s11356-022-23014-8>, 2023.
- 830 Zhu, Z. Y., Wu, Y., Liu, S. M., Wenger, F., Hu, J., Zhang, J., and Zhang, R. F.: Organic carbon  
831 flux and particulate organic matter composition in Arctic valley glaciers: Examples from the  
832 Bayelva River and adjacent Kongsfjorden, *Biogeosciences*, 13, 975–987,  
833 <https://doi.org/10.5194/bg-13-975-2016>, 2016.